The Journal of Experimental Biology 200, 2523–2538 (1997)
Printed in Great Britain © The Company of Biologists Limited 1997
JEB1138

LOCOMOTION ON THE WATER SURFACE: PROPULSIVE MECHANISMS OF THE FISHER SPIDER *DOLOMEDES TRITON*

ROBERT B. SUTER[1,*], OREN ROSENBERG[1], SANDRA LOEB[2], HORATIO WILDMAN[3] AND JOHN H. LONG, JR[1]

[1]*Department of Biology, Vassar College, Poughkeepsie, NY 12604, USA,* [2]*Division of Biological Sciences, Cornell University, Ithaca, NY 14850, USA* and [3]*Department of Zoology, Duke University, Durham, NC 27708, USA*

Accepted 14 July 1997

Summary

Using kinematic and mechanical experiments, we have shown how fisher spiders, *Dolomedes triton* (Araneae, Pisauridae), can generate horizontal propulsive forces using their legs. This horizontal thrust is provided primarily by the drag of the leg and its associated dimple as both move across the water surface. Less important sources of resistance are surface tension and bow waves. The relative contributions of drag, surface tension and bow waves were examined in several different ways. In one experiment, we measured the forces acting on a leg segment as water flowed past it in non-turbulent flow; the bow wave was not present at leg relative velocities below 0.2 m s^{-1} and thus cannot play a role in thrust production at low leg speeds. In a second experiment, we varied the surface tension by altering the concentration of ethanol from 0 % to 9 % in the experimental water tank. At a constant dimple depth, force varied little with changes in surface tension, a result consistent with the hypothesis that drag is the primary source of resistance. In addition, however, as surface tension decreased from 0.072 to 0.064 N m^{-1}, the power exponent of the relationship between force and velocity (as measured by the exponent of the power function relating the two variables) increased; at lower surface tensions, down to 0.054 N m^{-1}, the power exponent of the relationship between force and velocity decreased. These results suggest an influence of surface tension (albeit still secondary to drag) in generating horizontal resistance to leg movement. We also measured flow disturbance in the water downstream from a leg segment and confirmed that, even at velocities well below 0.2 m s^{-1}, the leg-cum-dimple transferred momentum to the water, which is a clear indication that drag is a contributor to the resistance encountered by a spider's leg. Finally, modeling the leg-cum-dimple as a circular cylinder generates values of drag that account for 75–98 % of the measured leg force when the dimple is 0 or 1 mm deep. These results not only elucidate the primary mechanism of propulsion for *D. triton* and other similar-sized arthropods, such as adult water striders (Gerridae), but also suggest that the formerly enigmatic locomotion of very small water-walking organisms (e.g. first-instar water striders) can be understood in the same way.

Key words: locomotion, aquatic propulsion, drag, drag-based locomotion, spider, *Dolomedes triton.*

Introduction

While experimental studies of legged locomotion on land have led to important generalizations regarding power requirements, gait transitions, maximum velocities and the effects of body size (e.g. Alexander, 1977, 1989; Blickhan and Full, 1993; Farley and McMahon, 1992; Farley and Taylor, 1991; Fedak *et al.* 1982; Full, 1990; Full and Tu, 1991; Full *et al.* 1995; Kram *et al.* 1997; Schmidt-Nielsen, 1984), the mechanical principles governing legged locomotion on the surface of the water remain relatively unexplored (Denny, 1993; Vogel, 1994). A notable exception to this dearth of information is work on basilisk lizards, *Basiliscus basiliscus*, of 2–200 g body mass, which support themselves on the water surface by using their feet to generate upward forces from surface impact ('slap') and the formation of an air cavity ('stroke') (Glasheen and McMahon, 1996*a*,*b*). This vertical slap-and-stroke mechanism, however, is unlikely to be used by the small (body mass <1 g) arthropods that propel themselves on the water surface using primarily horizontal leg movements. Some other physical phenomena must be at work, and experimental elucidation of the primary propulsive mechanism is the goal of this study.

For legged arthropods moving horizontally on land, the feet produce a friction force that transfers momentum from the animal to the substratum, accelerating both horizontally (in opposite directions). This propulsive force varies with changes in behavior. During running, 3.1 g death-head

*e-mail: suter@vassar.edu

cockroaches, *Blaberus discoidalis*, produce single-leg, horizontal ground reaction forces of 0.005 N; during righting, those forces increase to 0.034 N (Full *et al.* 1995). Larger still were the peak static forces, 0.160 N, produced by the metathoracic leg as the animal attempted to squeeze through a constricted opening (Full and Ahn, 1995). When adjusted for body mass (kg), these measurements provide an empirical basis for the possible range of horizontal forces (1.6–51.6 N kg^{-1}) that might be measured in arthropods of different sizes moving on the water surface.

A few groups of uniramian arthropods, notably water striders (Hemiptera, Gerridae) and fisher spiders (Araneae, Pisauridae), inhabit the surface of fresh water and locomote using feet supported but not wetted by the water surface. While the locomotion of water striders and similar insects has been studied descriptively (Anderson, 1976; Bowdan, 1978) and ethologically (Barnes and Barth, 1991), the mechanics of moving on the water surface has not been explored, except for some theoretical ruminations (Denny, 1993; Vogel, 1994) and cinematographic analyses (Anderson, 1976). The water-surface locomotion of the fisher spider *Dolomedes* sp. has been described in general (McAlister, 1959) and with regard to the variety of modes used (Deshefy, 1981), the details of the stepping patterns during rowing (Shultz, 1987) and the special conditions surrounding prey capture (Gorb and Barth, 1994). In spite of these efforts, we have no experimental data, and no single-leg force measurements, with which to test theoretical models of propulsion on the water surface.

The locomotion of a water strider or a fisher spider on the water surface is interesting for two additional reasons. First, the same hydrophobicity of the animal's exoskeleton and cuticular hairs that makes possible support of the animal by the water's surface tension also makes terrestrial-style locomotion difficult on the water surface. The very small amount of interaction between water molecules and the waxy molecules of the animal's surface reduces friction to a small fraction of the friction that would anchor the animal's foot to a solid substratum. Second, the weight of the animal, when supported by the water's surface tension, pushes the points of contact downwards, creating dimples in the water surface. When the legs are moved backwards to thrust the body forwards, it is the legs with their accompanying dimples that move backwards, not just the legs themselves. In that respect, one might want to consider the leg-cum-dimple to be hull-like in its interaction with the fluid medium (Fig. 1).

Thus, the locomotion of a water strider or fisher spider across a surface with which it has little micro-scale contact must depend upon the ability of the rowing legs to encounter or create resistance to their motion. Three possible mechanisms of resistance are presented below. In each case, the mathematical relationships are provided not for calculation of the predicted forces, but for the purpose of making testable predictions about how the water's resistive force should vary with experimental manipulation of the leg-cum-dimple, its motion and the properties of the fluid.

Bow wave resistance

As a hull moves at constant velocity through the water surface, it generates a standing bow wave that offers resistance to its forward motion. If the leg-cum-dimple operates as a hull, the resistance to the motion of a leg may result from the formation of a bow wave and the water surface's tendency to flatten under the influence of gravity and capillarity (Fig. 2A). For water striders, Denny (1993) stated the hypothesis as follows: "The answer appears to be

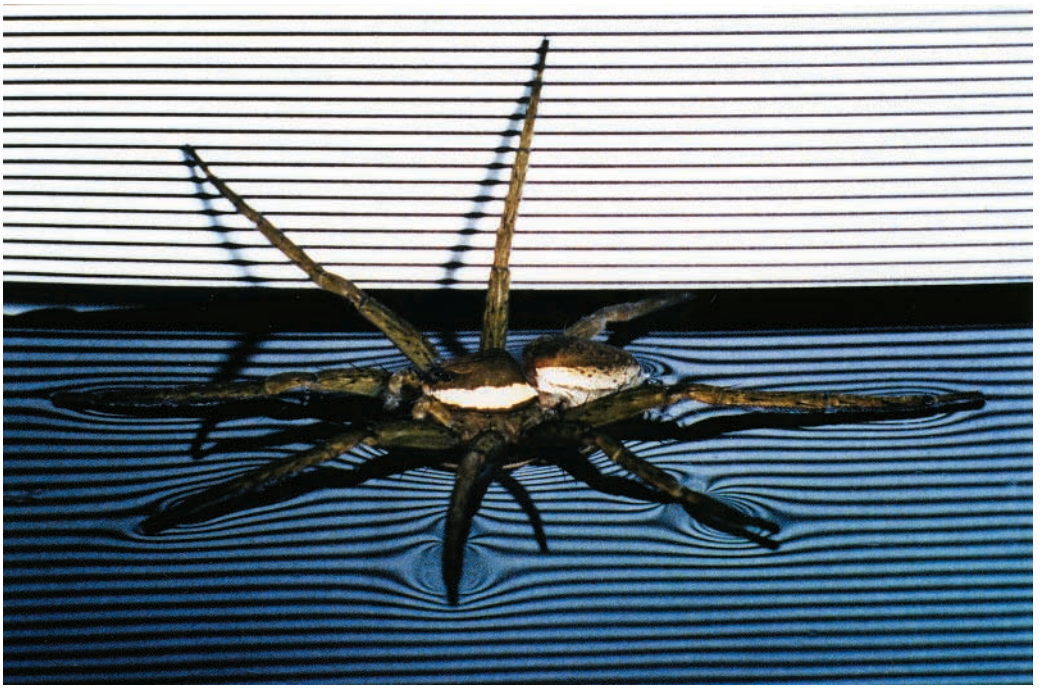

Fig. 1. A female fisher spider, *Dolomedes triton*, supporting most of its weight (6.9 mN, 0.7 g) on the surface of distilled water. Left lateral view, with the propulsive legs, II and III, shown in the foreground and elevated in the background indicating their relative length and taper. The horizontal lines on the vertical background (7.4 lines cm^{-1}) are reflected in the water surface; note that the distortions in the lines indicate depressions – dimples – made by the distal portions of the legs on the water surface.

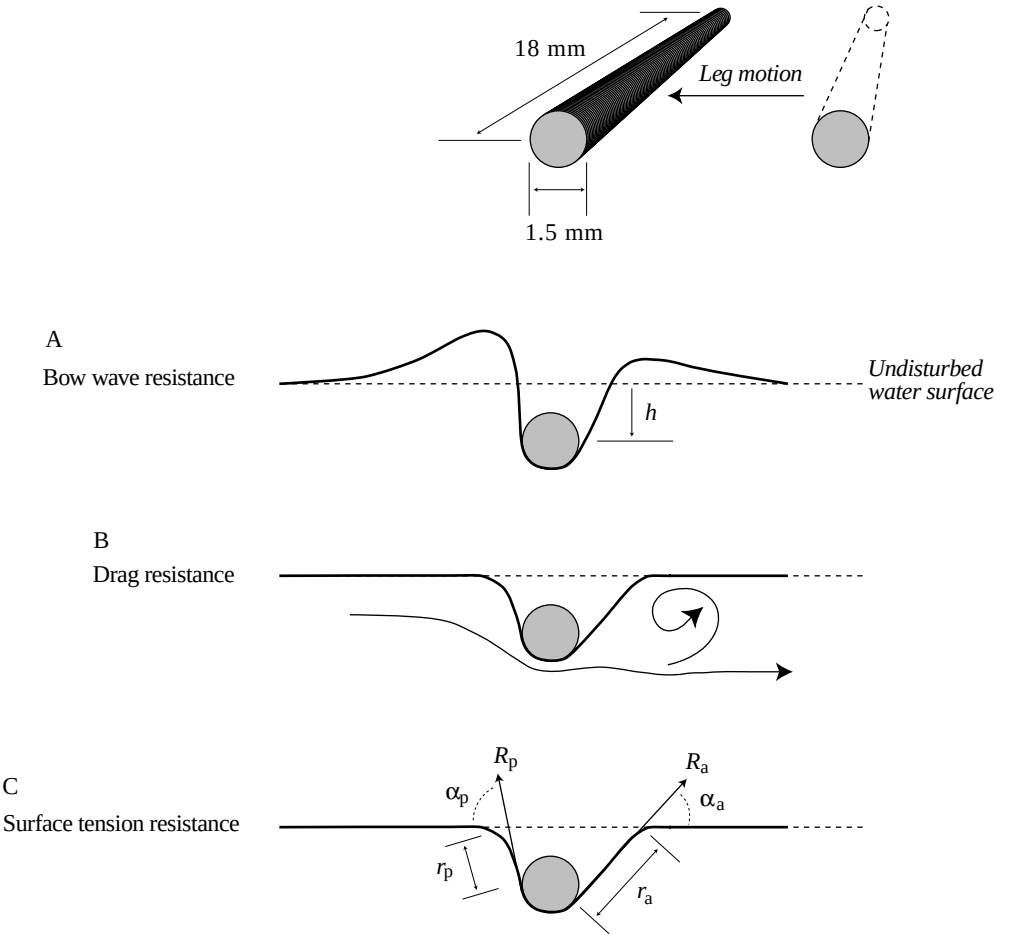

Fig. 2. Hypothetical sources of resistance for a leg generating thrust at the water surface. (A) Waves: the resistance is provided by a bow-wave that forms at the posterior edge of the leg and dimple as the leg sweeps backwards (*h*, dimple depth). (B) Drag: the leg and dimple experience resistance due to drag from the fluid through which they are moving. The arrows indicate the direction of flow of the fluid. (C) Surface tension: the movement of the leg causes a distortion in the shape of the dimple and thereby creates a horizontal component to the normally vertical surface tension vector. r_a and r_p, anterior and posterior distances from surface to leg contact; R_a and R_p, anterior and posterior resultants of surface tension forces; α_a and α_p, anterior and posterior angles formed between *R* and the water surface. See Table 1 for predictions of how thrust force, F_t, should change with changes in surface tension, γ, dimple depth, *h*, and leg speed, *U*.

that when the striders' middle pair of legs is swept backward, the legs create surface waves. The drag of moving against these waves provides the 'purchase' needed by the animal to skate across the water." The efficacy of this method of generating resistance depends upon the ability of the moving leg to generate a wave, and that ability is a function, in part, of the leg's velocity. Because of the interaction between surface tension, γ (in $N\,m^{-1}$ or $J\,m^{-2}$), and the force caused by gravitational acceleration, $\boldsymbol{g}$ ($m\,s^{-2}$), which, respectively, form small capillary and larger gravity waves, no waves at all will be produced below a minimum hull speed, c_{min} (Denny, 1993):

$$c_{min} = \sqrt{2\sqrt{\frac{\boldsymbol{g}\gamma}{\rho}}}\ , \qquad (1)$$

where ρ is the density of the water ($kg\,m^{-3}$). If γ is $0.0728\,J\,m^{-2}$ (pure water at 20 °C) and ρ is $998\,kg\,m^{-3}$ (fresh water at 20 °C), then c_{min} is $0.23\,m\,s^{-1}$.

At steady leg speeds above $23\,cm\,s^{-1}$, when waves should theoretically appear, we expect the leg's bow wave to balance the horizontal pressure of the foot against the water. From Bernoulli's equation (Denny, 1993), at a constant relative velocity, *U*, the horizontal resistive force caused by the bow wave, F_w, is the quotient of the total fluid pressure on the leg-cum-dimple and its frontal surface area, S_f, the surface upon which the propulsive force is applied:

$$F_w = \frac{1}{S_f}\left(\frac{\rho U^2}{2} + \frac{2\pi^2 H\gamma}{\lambda^2}\right), \qquad (2)$$

where *H* is the height of the wave (m) from the trough of the dimple to the peak of the bow wave and λ is the wavelength (m), which is twice the length of the dimple, assuming that the wave is sinusoidal. Several other assumptions are required for the application of this theory (Denny, 1993): (a) hydrostatic pressure and flow velocity are the same at any point along the wave, (b) the effect of gravity on wave formation at this scale of λ is negligible, and (c) the no-slip condition at the water-solid interface does not exist. Given these assumptions, equation 2 predicts that if the leg-cum-dimple uses a bow wave for propulsive resistance, then F_w will increase in proportion to U^2, γ and the inverse of S_f (Table 1).

Drag resistance

As the leg-cum-dimple moves through the water surface, with or without a bow wave, it should experience a resistive force caused by drag, F_d (Fig. 2B), which in turn is caused by the difference in the fluid's pressure distribution and by the

Table 1. *Qualitative predictions of the three hypothetical mechanisms resisting the horizontal motion of the spider's leg*

Resistance mechanisms	Independent variables: *U*, flow velocity ($m\,s^{-1}$)	*h*, dimple depth (m)	γ, surface tension ($N\,m^{-1}$)
F_w, horizontal force caused by the bow wave (N)			
F_d, horizontal force caused by drag (N)			
F_s, horizontal force caused by surface tension (N)			

Note that each mechanism has a unique *set* of predictions.
For details of the mechanisms, see text.

fluid's viscosity (Vogel, 1994). At Reynolds numbers (*Re*) above unity, F_d is proportional to U^2, S_f and the frontal coefficient of drag, C_{df}, a dimensionless factor that accounts for complex effects of shape and varies with changes in *Re*:

$$F_d = 0.5\rho S_f C_{df} U^2 . \quad (3)$$

Note that, while both F_w and F_d are proportional to U^2 (compare equations 2 and 3), F_w is inversely and F_d is directly proportional to S_f (S_f increases with *h*, see Table 1 and Fig. 2). It is also important to note that spider legs operate in a range of *Re* ($10<Re<10\,000$) in which C_{df} varies with *Re*, a situation that makes difficult the accurate calculation of F_d for even simple shapes (Vogel, 1994).

Surface tension resistance

While surface tension, γ, undoubtedly supplies much of the vertical resistance to hold a stationary insect upon the water surface (Denny, 1993), it may also supply horizontal resistance for propulsion (Vogel, 1994). When the leg-cum-dimple is at rest, the horizontal components, $F_{s,a}$ and $F_{s,p}$, of the resultant forces, R_a and R_p, due to surface tension at the anterior and posterior margins of the leg, respectively, are balanced because the dimple is symmetrical (Vogel, 1994). When the leg-cum-dimple moves horizontally, the dimple may be tilted or reconfigured (Fig. 2C) such that the horizontal forces, $F_{s,a}$ and $F_{s,p}$, are unbalanced, thus providing a net forward or backward force for resistance or pulling of the moving leg. The net horizontal force due to surface tension, F_s, is thus the sum of $F_{s,a}$ and $F_{s,p}$. The magnitude of the horizontal forces depends on the orientation of R_a and R_p, relative to the undisturbed water surface, measured by the anterior and posterior tilt angles, α_a and α_p, respectively (Fig. 2C), measures which permit the following formulations:

$$F_{s,a} = l\gamma\cos\alpha_a \quad (4)$$

and

$$F_{s,p} = l\gamma\cos\alpha_p , \quad (5)$$

where *l* is the length (m) of the leg interacting with the surface. Since the tilt angles depend on the shape of the dimple (Fig. 2C), we can approximate α_a and α_p from the dimple depth, *h* (m), and the distances (m), r_a and r_p, from the leg's surface contact points in the anterior and posterior directions, respectively:

$$\alpha_a = \sin^{-1}\left(\frac{h}{r_a}\right) \quad (6)$$

and

$$\alpha_p = \sin^{-1}\left(\frac{h}{r_p}\right) . \quad (7)$$

By combining equations 4 with 6 and 5 with 7, it is clear that the net horizontal force due to surface tension, F_s, depends on the shape of the dimple, as described by the ratio of *h* to r_a and r_p. Thus, in order for surface tension to generate a resistive force (coded with a positive sign) for the moving leg, we must have $h/r_a<h/r_p$, which results in $\alpha_a<\alpha_p$ (equations 6 and 7), $F_{s,a}>F_{s,p}$ (equations 4 and 5) and, finally, a net positive F_s. With increasing distortion caused by increasing flow velocity, *U*, we predict that r_a and r_p will increase and decrease, respectively, when *h* and γ are held constant, resulting in a greater F_s. If *U* and γ are held constant as *h* increases, and we assume that the dimple increases in size isometrically, with no change in the net difference between $F_{s,a}$ and $F_{s,p}$, F_s will be independent of *h*. When *U* and *h* are held constant, F_s should change in direct proportion to surface tension, γ (for a summary, see Table 1).

Another possible consequence of surface tension that we initially considered was assymetry in γ as the leg moved and distorted the surface. If, by pushing on the surface, the leg were able to compress the leading and stretch the trailing surface, we might expect $F_{s,a}$ and $F_{s,p}$ to be unbalanced, thus providing a net positive F_s. If the surface behaved like a thin rubber

membrane, this might be a reasonable hypothesis. However, the comparison with an elastic membrane is unjustified on theoretical grounds and, because no new water surface is actually created under these circumstances, this hypothesis is untenable (Denny, 1994).

Any of these hypothetical sources of resistance, alone or in combination, might account for the ability of fisher spiders to propel themselves horizontally on the water surface. Thus, for a single leg, the thrust force, F_t, is the sum of the three resistive forces:

$$F_t = F_w + F_d + F_s \, . \quad (8)$$

Note that this equation is only applicable to steady-state situations when the leg has achieved a constant velocity. Unsteady effects – such as the acceleration reaction and creation of additional interface water surface area – are likely to play a role at the beginning and end of the propulsive stroke, but are unlikely to be important during the constant-velocity leg motions during the middle of the stroke (see Results).

In the experiments described below, we sought to determine, by measuring F_t on an isolated leg, which of these sources of resistance (equation 8; Fig. 2; Table 1) was most important in the aquatic locomotion of the fisher spider, *D. triton*. To accomplish this, we manipulated three independent variables: U, the velocity of the foot moving across the water surface, h, the depth of the leg-cum-dimple, and γ, surface tension. In order to determine the physiologically relevant range of leg velocities and locomotor forces for our isolated leg experiments, we also measured the locomotor kinematics of live fishing spiders. Finally, we measured the presence of waves and flow pattern disturbance as supplementary evidence regarding the importance of a resistive bow wave (equations 1 and 2) and sub-surface momentum transfer *via* drag (equation 3), respectively.

Materials and methods

Spiders

Dolomedes triton (Walckenaer) (Fig. 1; Araneae, Pisauridae) are large spiders (adult females: body mass $\leqslant$1.2 g, leg length $\leqslant$5 cm) that inhabit marshes and the edges of ponds and streams throughout much of North America (Gertsch, 1979). The subjects for these experiments were collected from small ponds in Mississippi, USA, and held in our laboratory (at 22–25 °C) in 4 l plastic aquaria containing fresh water (approximately 2 cm deep) and an inverted clay flower pot to provide a solid substratum. We fed the spiders assorted insects and changed their water approximately once a week. We used 19 intact spiders of a range of instars in the videographic portion of this study. The exuviae of newly molted adult spiders and leg segments of killed adults were stored in dry air; from this sample, we selected distal portions (tarsus plus tibia) of legs III, varying in length from 10 to 18 mm and in maximum (proximal) width from 1 to 1.5 mm for the isolated leg segment experiments. These segment lengths roughly approximated the lengths of the propulsive (in contact with the water) portions of the legs of the intact spiders that we video-taped moving across the water surface (see Results). All observations and experiments were conducted at laboratory temperatures between 22 and 25 °C.

Kinematics of live spiders

Because most of the motion involved in the spiders' movement across the surface of water occurs in the horizontal plane, we video-taped their locomotion from directly above. The arena enclosing a test spider consisted of a white porcelain-surfaced tray, a smooth, circular plastic barrier to prevent the spider's escape, and a layer of water at least twice as deep as the deepest dimple we had observed for a spider of the size of the test spider. The arena was lit with an incandescent projector bulb, mounted at 45 ° above and to one side of the video-taped part of the arena, which provided an intense point source. We adjusted the video camera's lens aperture to obtain sufficient depth of field to allow both the spider and its shadow (on the porcelain surface of the arena) to be in sharp focus.

During a trial, we placed the test spider in the arena, recorded its movements at 1000 images s^{-1} using a high-speed video system (Kodak, model EktaPro EM-1000) and stored the images in S-VHS format (Sony, model 9500 MDR). For analysis, we used only motion sequences that met the following criteria: (1) the spider's initial velocity was between 0 and 0.02 m s^{-1}, (2) the motion of the spider during the filmed sequence was in a straight line, (3) the spider was in contact with the water at all times (i.e. it did not leap or gallop), and (4) the sequence included both the power stroke and enough of the subsequent glide to allow an accurate determination of the rate of deceleration.

We analysed the spider's motion, image by image, in the horizontal plane by overlaying each digitally paused video frame (Sony, model 9500 MDR) with a computer-generated x–y cursor grid (National Institutes of Health software Image, version 1.55 f) by means of a video scan convertor and synchronizer (Mass Microsystem model Colorspace II installed in an Apple Corporation computer, model Centris 650). Coordinates of the anterior or posterior tip of the body were manually digitized either every 1 ms (for small spiders) or every 5 ms for the duration of a propulsion episode (from the beginning of the power stroke of legs III to the termination of the passive deceleration). We used these coordinates to analyze the displacement of the spider through time; acceleration of the spider was calculated as the slope of portions of the velocity *versus* time relationship, where each velocity was calculated discretely as the quotient of the change in displacement and the change in time increment (Fig. 3). Accelerations were calculated for the parts of the power and glide phases during which the change in velocity with time was approximately linear (Fig. 3). Newton's second law ($F=ma$) allowed us to calculate the average net force exerted by the spider's legs during the power phase and the average resistance exerted by the water during the glide phase.

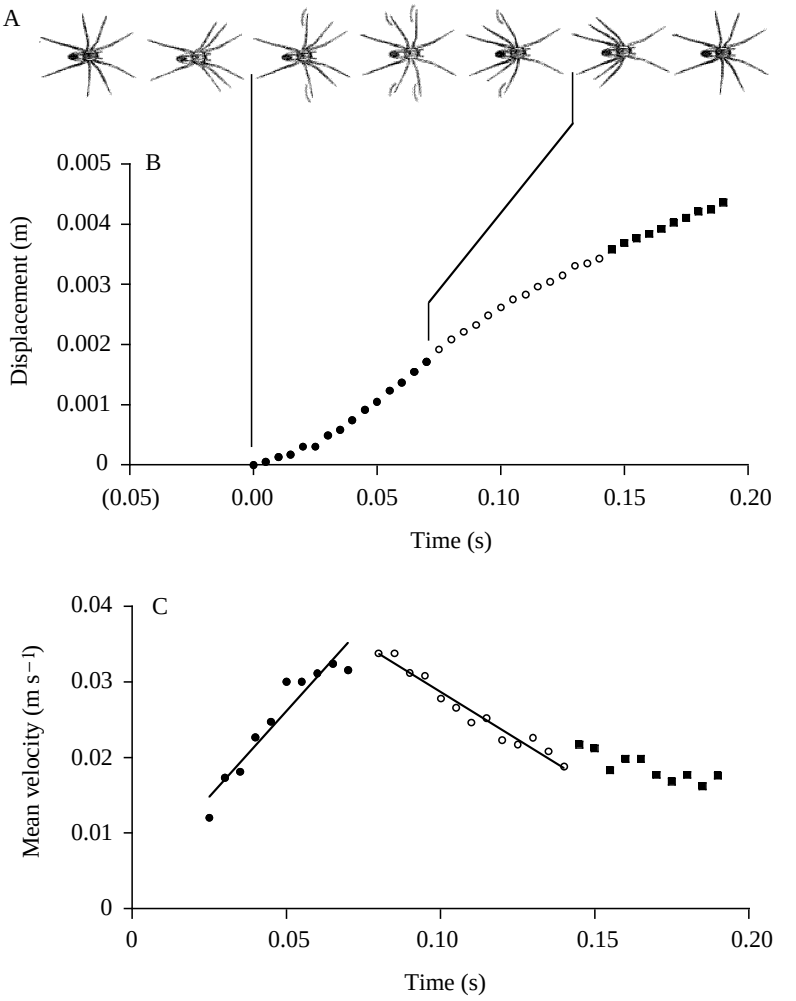

Fig. 3. Measuring body accelerations in living fisher spiders. (A) Complete propulsive stroke including both the power strokes of legs II and III and the glide phase; the drawings are from digitized video images. During the propulsive stroke, legs III are active before legs II, and there is a brief period during which all four propulsive legs are active. The edge of the dimple is indicated in some images. (B) Displacement of the body with respect to time during the power (●) and glide (○ and ■) phases of the full propulsive stroke (typical results). Different symbols are defined below. (C) Velocities (shown as five-point running averages of the displacement data) and accelerations (slopes of straight lines fitted by the least-squares method to the velocity data) for the power (●, $0.454\,m\,s^{-2}$) and glide (○, $-0.252\,m\,s^{-2}$) phases of the propulsive stroke. The rate of decrease in velocity during the second part of the glide (■) was obviously different from the initial deceleration and so was omitted from the analysis.

Using the same experimental apparatus and analytical techniques, we measured the angular velocity of the propulsive legs II and III, relative to the longitudinal axis of the spider's body, during the power stroke (Fig. 4). We used the angular velocity to calculate the velocity of the leg relative to the cephalothorax at known distances from the leg's attachment to the spider; direct measurement of leg tip velocity was not possible during the power phase because, in many trials, the image of the leg tip was invisible in the refractive shadow of the leg-cum-dimple.

Force transduction

To measure forces on an isolated leg III in the horizontal plane, we used a horizontal balance to which a leg segment was attached (Fig. 5). At the core of the balance was an electronic clinometer (Applied Geomechanics Inc., model 900

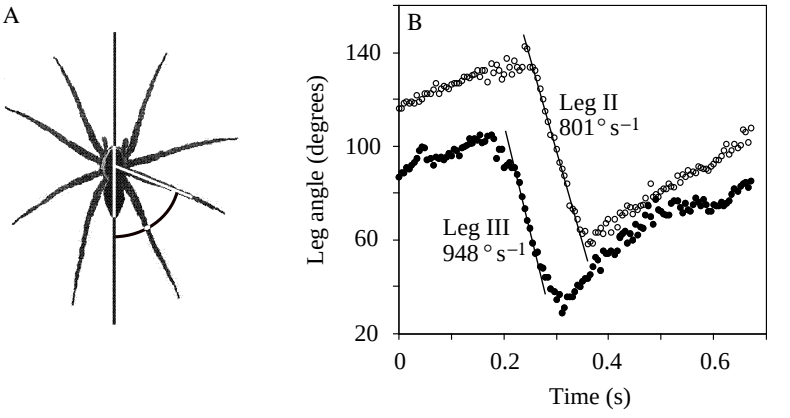

Fig. 4. Measuring leg tip velocities in living fisher spiders. (A) Drawing from a digitized image of *D. triton* at rest, illustrating the geometry of angular measurements used to generate the data shown in B. (B) Straight lines fitted to the linear portions of the power strokes of legs II (○) and III (●) provided angular velocity information used in calculating the velocities of the dimple-forming parts of the legs relative to the spider's body. In the example shown here, the angular velocities resulted in leg tip velocities of $0.322\,m\,s^{-1}$ for leg II (length, *l*, 0.023 m) and $0.347\,m\,s^{-1}$ for leg III (*l*=0.021 m).

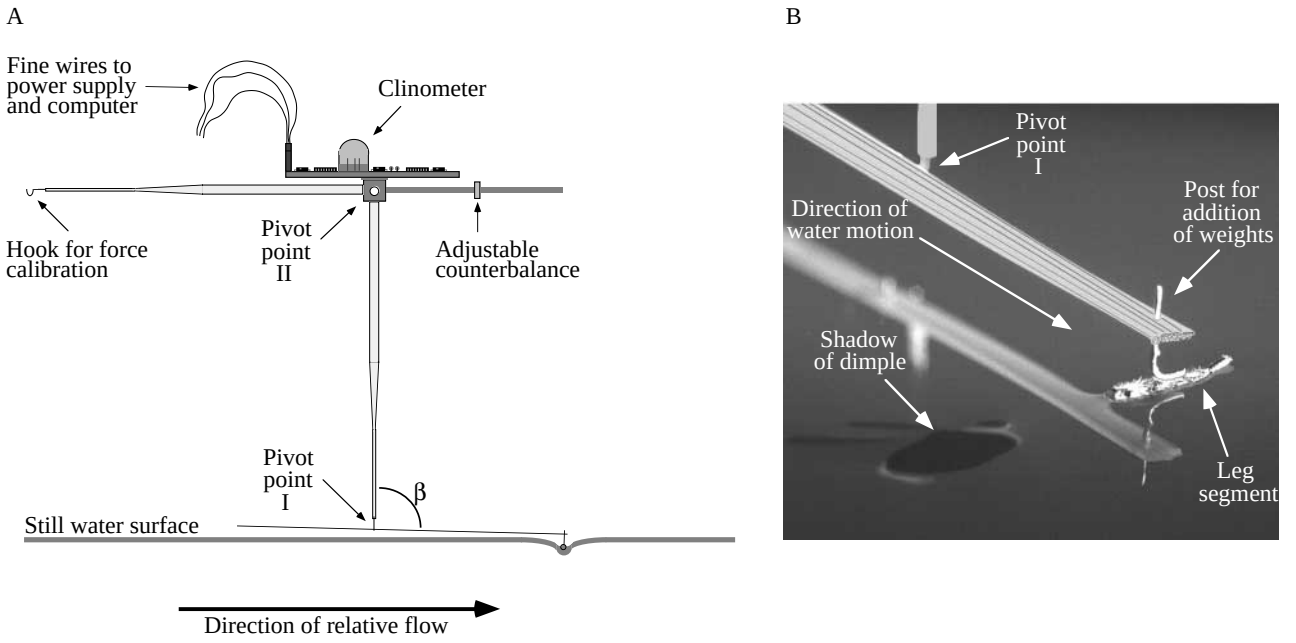

Fig. 5. Measuring force, F_t , on isolated leg segments. (A) Diagram of the balance used to measure horizontal forces on leg segments resting on the water surface. Water flowing past the leg segment caused a horizontal displacement of the segment and the almost horizontal arm to which it was attached. Because of the pivot (pivot point I), the horizontal displacement increased angle β but did not change the spatial relationship between the leg segment and the water. The horizontal displacement of the segment and its attachment arm caused the clinometer and its vertical and horizontal arms to rotate around pivot point II to a degree directly and linearly proportional to the force exerted on the leg segment. (B) Close-up of a leg segment on the water surface (photograph, oblique view). Note that the long axis of the leg is oriented perpendicular to the direction of water flow.

Biaxial Clinometer) with a resolution of 0.01 ° (1.75×10^{-4} rad). The clinometer, attached to a pair of 25 cm tubular glass arms, could pivot around a horizontal axis that was perpendicular to the direction of water flow (‘pivot point II’ in Fig. 5). Because the leg segment was attached to a balance beam and not rigidly to the vertical arm of the balance (‘pivot point I’ in Fig. 5), the force pushing the leg segment down onto the surface of the water was always constant during a test. The force could be manipulated by adding weights to the leg end of the balance beam. The addition of weights to the weight post at the leg end of the balance beam caused an increase in the depth of the dimple, *h*, formed by the leg and its interaction with the water surface. We calculated *h* in still water by subtracting the height of the weight-post (measured using a micrometer caliper) with a test weight added from the height of the post with no weight added. The leg segment was judged to be at h=0 when, by close visual inspection in still water, the segment produced no visible dimple; note, however, that the irregularity of the leg surface (caused by leg hairs) meant that whenever the segment was in contact with the water there was some distortion of the water surface.

The distilled water or ethanol solution (see next section) moving past the leg segment contained no detectable flow disturbance, and so effectively replicated the still surface of a pond upon which a fisher spider would propel itself. This was accomplished because the water moving past the stationary leg was contained in a shallow, horizontally rotating cylinder and was moving with the same angular velocity as the cylinder itself. With respect to the container holding it, the water was not moving at all; but with respect to the leg segment on the surface, the water was moving at a velocity proportional to the angular velocity of the cylinder and the distance of the segment from the axis of rotation. The inside circumference of the cylinder (diameter 65 cm, depth 3 cm) was lined with a 1 cm thick layer of aquarium filter wool that effectively absorbed surface waves that reached the perimeter and therefore prevented the reflection of waves back into the experimental area. The cylinder rested on top of a turntable powered by a variable-speed d.c. motor (Bison Gear and Engineering Corporation, model 507-01-127). The only connection between the motor and the turntable was a pair of elastic bands, one to each of two speed-reduction pulleys, resulting in nearly vibration-free rotation of the cylinder and the fluid it contained. In practice, we made speed changes in small increments and collected force data only after the turntable had been at the new test speed for at least 1 min, allowing time for the water to attain the same angular velocity as the cylinder.

The output of the clinometer (in V) was digitized using an analog-to-digital (A/D) convertor (National Instruments Corporation, model NB-MIO-16L) driven by a custom-designed program (National Instruments software LabView 3) on a microcomputer (Apple Corporation, model Centris 650). The A/D converter also sensed voltage peaks in the

output of an infrared tachometer mounted under the turntable. The software program converted the clinometer's voltage into total or thrust force, F_t, and calculated the relative velocity of the water, U, past the leg segment, which was located approximately 24 cm from the center of the cylinder. For each experiment, consisting of a given leg length l, dimple depth h, and surface tension γ, scatter plots of force as a function of water velocity were fitted using power curves (CA-CricketGraph software III v. 1.5.3), since we anticipated that F_t would be proportional to U^2 (see equations 2 and 3).

The force transduction method outlined above measured forces at constant U and so is only appropriate in this study if the propulsive stroke of the live spider has a constant velocity. Because the angular velocity of a leg during most of its power stroke is constant (Fig. 4), the velocity of the part of the leg that is in contact with the water surface is also constant relative to the spider's body. Although the spider's body is being accelerated during the power stroke, its velocity is always much less than that of the leg tips (compare Figs 3 and 4). Thus, the velocity of the leg tips relative to the spider's body approximates (with some exaggeration) the velocity of the leg tips relative to the water, and the velocity of the leg tips relative to the water is nearly constant. For these reasons, we can disregard the acceleration reaction and other unsteady mechanisms (Daniel, 1984).

Altering surface tension

In order to test the the predictions of the bow wave and surface tension hypotheses (see equations 2 and 4–7), we altered γ by adding ethanol to the distilled water. Ethanol in aqueous solution affects both γ and the kinematic viscosity of the solution: as the concentration of ethanol rises from 0 % (distilled water) to 9 %, γ falls from 0.072 N m^{-1} to 0.054 N m^{-1} and kinematic viscosity, ν, rises from 1.01×10^{-6} m^2 s^{-1} to 1.59×10^{-6} m^2 s^{-1} (Chemical Rubber Company, 1993). Note that the isolated leg experiments were performed at Reynolds numbers, Re, that ranged from approximately 30 to 1100 (for details, see below).

We measured horizontal forces, F_t, on an 18 mm (length) leg segment (see previous section) while increasing the concentration of ethanol in 1 % steps from 0 % (distilled water) to 9 %, yielding values of γ of 0.0716, 0.0696, 0.0676, 0.0657, 0.0637, 0.0617, 0.0597, 0.0578, 0.0558 and 0.0538 N m^{-1}. We avoided using higher concentrations of ethanol because changes in the hydrophobicity of the leg segment's surface might result, since segments held in 30 % ethanol for an hour lose their ability to form a dimple in the water surface, an indication that hydrophobicity has been lost. To keep experimental conditions as uniform as possible, we left the leg segment in place during changes in ethanol concentration. We made the changes by removing a small volume of the test solution and gradually replacing that volume with the same volume of a dilute ethanol solution the concentration of which had been calculated to increase the test solution's concentration by 1 %. To determine whether significant alcohol evaporation would occur during the 2–3 h needed for a full ethanol series, we measured γ (using the capillary rise method) of a 10 % ethanol solution in the test chamber over 3 h. We could detect no change in surface tension, and concluded that evaporation of ethanol would not significantly affect our results. We used only a single length (18 mm) of a single leg because measurements of multiple leg lengths are not necessary to test the predictions of our hypotheses and because the use of a single leg for all trials eliminated the small variations in force that could have arisen from small variations in leg shape, surface contour and hairiness.

Wave analysis

To test the predictions of equation 1, and hence the relative importance of F_w, we needed to determine at what relative water velocity waves first appeared and whether their appearance was abrupt or gradual as water flowed past an

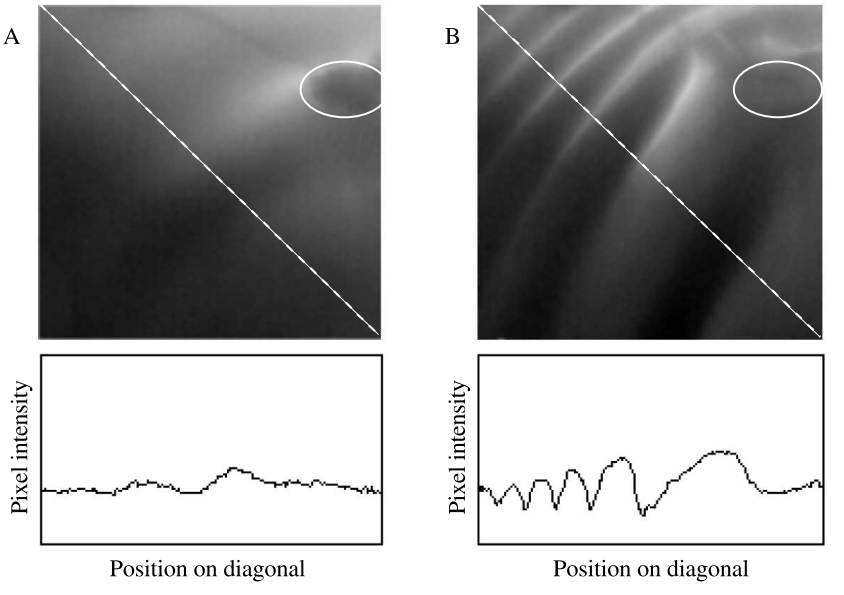

Fig. 6. Detecting surface waves. Surface waves form at the upstream and downstream sides of a *D. triton* leg segment moving across the water surface at relative velocities greater than 0.2 m s^{-1}. The wave index is the standard deviation of relative pixel densities (lower panels) measured along the diagonal (white broken line) of a digitized image of wave shadows (upper panels). The ovals in the digitized images indicate the approximate locations of the shadow of the leg segment. These images yielded wave indices of 6.0 (A) and 16.1 (B).

isolated leg segment. Note that we did not need to know the absolute magnitudes of the waves. To make these determinations, we used a 35 mm camera and an electronic flash to photograph (from above) the bottom of the rotating cylinder on which was cast the shadow of a 12 mm (length) leg segment as it rested (h=0.5 mm) on the distilled water surface. As waves appeared, the surface distortion caused refraction of the light from the electronic flash and that, in turn, caused wave shadows to appear on the bottom of the cylinder (Fig. 6). Twenty-six 35 mm photographs, taken at a variety of relative water velocities, were scanned (Epson ES-1200C) into a computer using software (NIH software Image v. 1.55f), and the pixel intensity of each image was measured along a standard transect running perpendicular to the wave crests and outside the leg's shadow. By measuring the standard deviation of pixel intensity along the transect, we generated an index of the waviness of the water surface, not a measure of wave amplitude *per se*.

Flow pattern disturbance

One indicator of the presence of sub-surface drag force (equation 3) is the disturbance of the flow pattern around the sub-surface structure (Vogel, 1994). Specifically, by disturbance we mean evidence that the momentum of the fluid perpendicular to the flow has been altered, which indicates, in the case of our isolated leg experiments, that the leg-cum-dimple is removing momentum from the sub-surface flow (Fig. 2B). The level of disturbance was measured as the amount of change in a pattern of light reflected by the surface of the water (Fig. 7). First, we mounted a card perpendicular to the distilled water surface in the turntable, positioned so that the reflection (on the water surface) of the horizontal lines on the card could be photographed by a 35 mm camera (as in Fig. 1). The card, the camera's film plane and the water that had just passed under and around the leg-cum-dimple were parallel to one another. As a result, distortions in the water surface caused by sub-surface flow disturbance were visible as distortions in the reflections of the horizontal lines. Photographic images were digitized in the same manner as were those for the wave index measurements (see previous section) and were then analysed using NIH software (Image v. 1.55f) as described in Fig. 7.

Statistical design

To test the hypothesis that F_t is a function of U, h and γ, we conducted a modified analysis of covariance (ANCOVA) on our data from the isolated leg experiments (Sokal and Rohlf, 1981). First, for each experimental trial, with a constant h and γ over a range of U from 0 to 0.2 m s^{-1}, we regressed F_t onto U using a power fit of the following form (CA-CricketGraph III software v. 1.5.3):

$$y = cx^b \,, \tag{9}$$

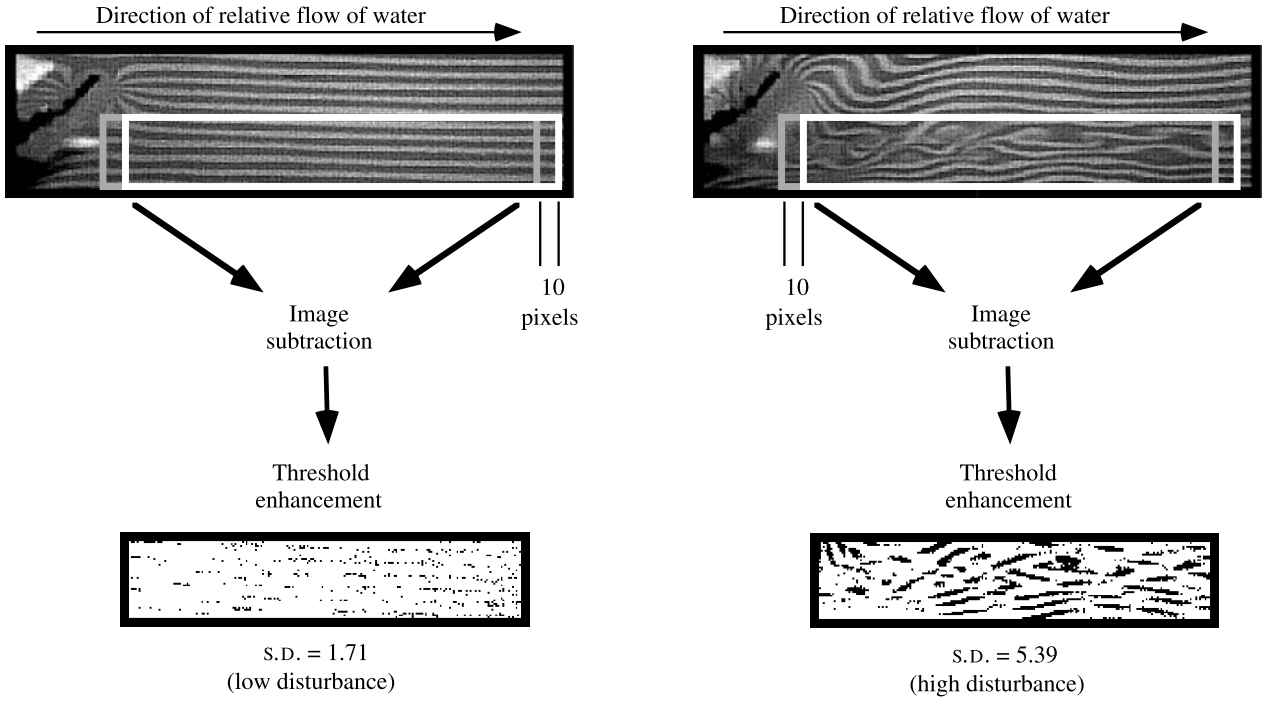

Fig. 7. Measuring flow disturbance. Two examples, produced by analysis of digital images, illustrate how the index of flow disturbance is measured. The two frames at the top show digitized images of the water surface just downstream from the leg segment, which is at the left in each image. The horizontal lines are reflections of horizontal lines on a vertical card just beyond the view of the camera. Distortions in the water surface cause visible distortions in the reflections. These distortions are quantified first by subtracting two subsets of the image, one displaced 10 pixels to the right of the other, and second by measuring the pixel intensity variation in an enhanced version of the difference image. The variation, represented as a standard deviation of pixel intensity, served as an index of flow disturbance.

where y is F_t, c is the regression constant, x is U, and b is the regression exponent. We chose this relationship based on the *a priori* expectation that F_t would be an exponential function of U, with b having values between 1 and 2 (Vogel, 1994). Note that b is also the logarithmic slope when equation 9 is log-transformed. For each experimental trial, b then becomes the single response variable that summarizes the relationship between F_t and U.

To test for the homogeniety of slopes between treatments, the first stage in ANCOVA, the variance in b was tested in a two-way analysis of variance (ANOVA), with h and γ as the categorical independent variables, with 2 and 9 degrees of freedom (d.f.), respectively. Planned contrasts were made between categories within each independent variable. For h, we investigated whether the mean values of b differed between 0 and 1 mm, and between 1 and 2 mm. For γ, we investigated whether the mean values of b differed between neighboring values of γ and between the middle and end values (SAS Institute, v. 6.11).

Modeling drag from first principles

In addition to the experimental procedures described above, we also modified equation 3 to calculate drag of the leg-cum-dimple, reasoning that if drag were the primary propulsive force, approximations of F_d from first principles should approximate F_t on the isolated leg (see equation 8). The key to accurate drag estimates is an accurate measurement of the coefficient of drag, C_d, which varies as a function of the shape and Reynolds number, Re, of the object (Vogel, 1994). For simple objects, such as flat plates and circular cylinders, the relationship between C_d and Re is well known.

As the first step in calculating F_d , we estimated Re of the leg-cum-dimple. The ratio of inertial to viscous fluid forces, Re is calculated as the following dimensionless number:

$$Re = \frac{L_c U}{\nu} , \qquad (10)$$

where ν is the kinematic viscosity ($m^2\,s^{-1}$) of the water and L_c (m) is the 'characteristic length' of the object, which is usually the object's largest dimension parallel to the flow. For the leg-cum-dimple, L_c was varied linearly with changes in h, from the leg's width (1.5 mm) at h=0 mm, to an intermediate value of the dimple width (3.5 mm) at h=1, to the maximum dimple width (5.5 mm) at h=2 mm. Re also varies with our experimental changes in ν; for fresh water, $\nu=1.01\times10^{-6}\,m^2\,s^{-1}$ at 20 °C; for the 9 % aqueous ethanol solution, $\nu=1.59\times10^{-6}\,m^2\,s^{-1}$ at 20 °C. Because we calculated F_d over a range of U from 0.025 to 0.20 m s^{-1}, Re varied from 38 to 733.

We modeled the surface of the dimple as half of a circular cylinder oriented with its long axis perpendicular to the flow. Using this simple model, we calculated the frontal coefficient of drag C_{df} as half of that given for a full cylinder (see Vogel, 1994):

$$C_{df} = 0.5(1 + 10.0Re^{-2/3}) . \qquad (11)$$

By substituting equation 11 into equation 3, we then have an equation for drag, and hence F_d :

$$F_d = 0.25\rho S_f U^2(1 + 10.0Re^{-2/3}) , \qquad (12)$$

where S_f is the frontal surface area of half a circular cylinder which, in this case, is one-quarter of the cylinder's total curved surface area:

$$S_f = \frac{\pi}{2} hl , \qquad (13)$$

where h is the dimple depth (radius) and l is the length of the leg. Note that for F_d when h=0 mm, we used an actual h of 0.0075 m, which is the radius of the leg, since the leg creates a dimple even though its mean height is 0.

Results

Living spiders

During the acceleration phases of surface locomotion by *D. triton*, the leg velocities and whole-body forces, derived from videographic measurements (Fig. 3) made on 19 spiders of different sizes, indicate that the spiders produced net leg tip velocities with means ranging from 0.16 m s^{-1} to 0.62 m s^{-1} (Fig. 8A) and mean forces in the range 0.008–0.327 mN during acceleration (Fig. 8B). In the acceleration phase, the forces were generated by the backwards sweep of the third and second pairs of legs (Fig. 3) but, because acceleration was approximately constant while legs III, then III plus II, and then II alone were providing thrust (Fig. 3), we could treat the system as if only one pair of legs was used throughout. Thus, the thrust produced per leg varied between 0.004 and 0.164 mN (the range given above divided by two). Because this forward force had to be the difference between the forward force generated by the legs and the backward resistance of the water on non-propulsive parts of the spider, the estimate of the force generated by each leg must be an underestimate.

During the trials, dimples of leg III were as deep as 3.5 mm, and the largest spiders often had more than 18 mm of each propulsive leg in contact with the water surface (although only the tip of the leg would have been at the maximum depth). Thus, the thrust estimates, F_t , based on data from an isolated leg segment of 18 mm length (see next section), underestimate the actual thrust that the legs of a spider should be able to generate.

Isolated leg experiments

At experimental values of U below 0.21 m s^{-1}, a bow wave, or a wave of any kind, was not detected, as indicated by the wave index (Fig. 9). At U of 0.21 m s^{-1}, waves appeared abruptly and, with increasing U, increased rapidly in amplitude and frequency. This result supports the prediction (Denny, 1993) that bow waves should not be available as a source of resistance to the leg at low U (equation 1). Because F_w cannot be operating at U<0.20 m s^{-1}, we restricted our experimental manipulations of h and γ to this lower range of U.

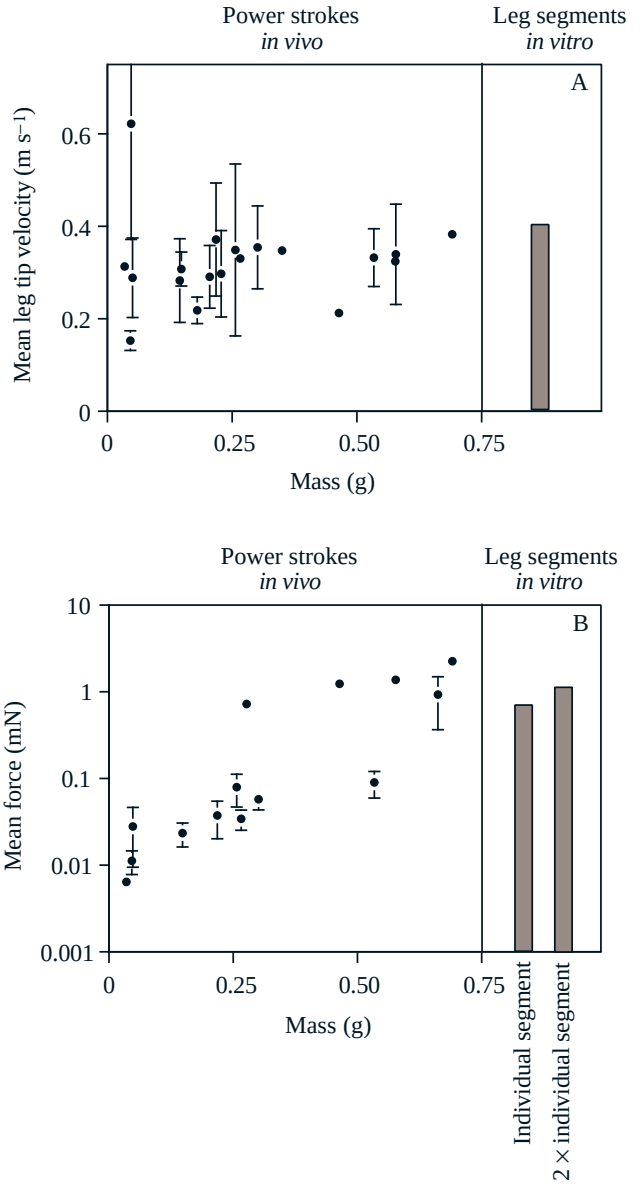

Fig. 8. Motion of living spiders. (A) Mean leg-tip velocities (± S.D.) as a function of body mass. Note that velocities *in vivo* ranged from means of approximately 0.16 to 0.62 m s^{-1}. Velocities used in the isolated leg experiments (bar) ranged from 0 to 0.40 m s^{-1}, a range that encompasses more than 75 % of the leg tip velocities observed *in vivo*. (B) Mean forces (± S.D.) as a function of body mass. Forces measured *in vivo* varied over more than two orders of magnitude, covering a range comparable to the actual forces measured on single leg segments (individual segment bar) and even more comparable to those measurements doubled (to simulate the simultaneous action of two propulsive legs, multiply the individual segment bar by a factor of two). Each value is plotted for a different individual.

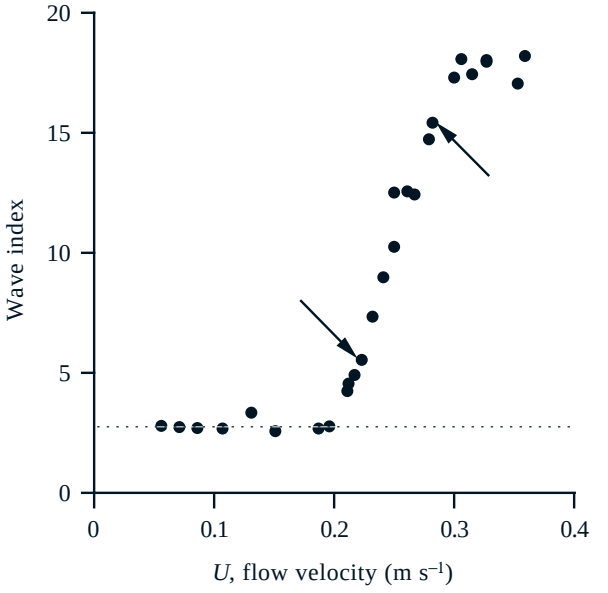

Fig. 9. Wave production as a function of flow velocity *U*. A wave index of 2.5 indicates no detectable waves (horizontal line). The abrupt increase in the wave index at approximately 0.21 m s^{-1} coincided with the abrupt appearance of surface waves on visual inspection of the water surface. The *in vivo* range of leg tip velocities usually exceeds 0.21 m s^{-1} (see Fig. 8A), but parts of a propulsive leg that are proximal to the leg tip move more slowly than the leg tip itself and, when in contact with the water but moving at less than 0.21 m s^{-1}, will not contribute to the production of waves. The arrows on the graph indicate data derived from the digitized images shown in Fig. 6. These data are derived from a single series of measurements on a 12 mm leg segment; the shape of the relationship, especially the abrupt rise from the baseline at velocities above 0.21 m s^{-1}, was also observed when measurements were made using shorter leg segments, using leg segments oriented perpendicular to the water surface, and using fine (diameter 0.05 mm) stainless-steel wire oriented perpendicular to the water surface.

The horizontal force, F_t, generated by an isolated leg segment (18 mm in length) and its associated dimple, as it moved across the water surface varied from 0 to 0.6 mN at relative leg velocities, U, of up to 0.2 m s^{-1} (Fig. 10). The relationship between F_t and U for each experiment (constant h and γ) produced a range of power curves with exponents (b in equation 9) varying from 1.601 to 2.135. This range of exponents includes the value of 2 predicted from the bow wave (equation 2) and drag (equation 3) resistance hypotheses. Note that the surface tension resistance hypothesis (equations 4–7) also predicts an increase in F_t with increasing U (see Table 1), although it is unclear what the exact relationship should be, since F_s depends on the exact shape of the dimple during the power stroke, and we did not measure this feature.

As revealed by ANOVA (Table 2), changes in both dimple depth, h, and surface tension, γ, significantly altered b. A comparison of the F-values of the two factors reveals that much more of the variance in b is explained by the variance in h than that in γ. Statistical comparisons (Table 3) indicate that with increasing dimple depth, h, from 1 to 2.0 mm, the power exponent, b, of F_t increases significantly (Fig. 11). This result is consistent only with the predictions of the drag resistance hypothesis (equation 3; see also Table 1). Statistical comparisons using ANCOVA (Table 3) also show that with

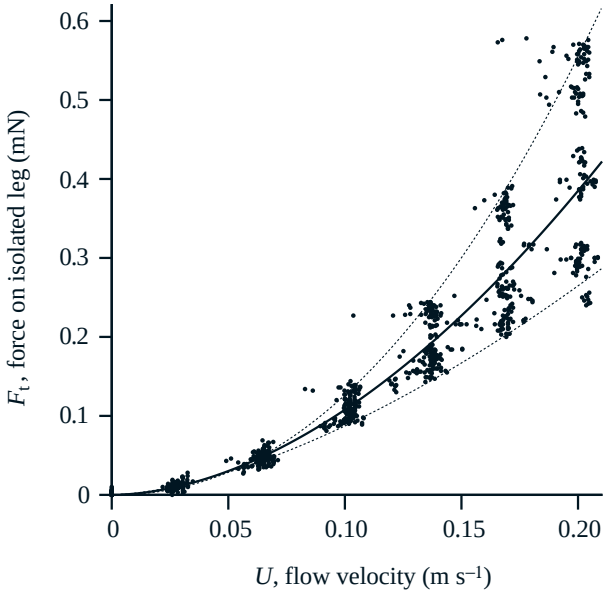

Fig. 10. Flow velocity and horizontal leg forces. Horizontal forces, F_t, on an isolated leg segment (18 mm in length) over a range of velocities U. When averaged over all the experiments that varied γ and h, the average relationship between F_t and U is $F_t=7.397U^{1.837}$ (solid line; N=1170 points; r^2=0.962). For individual experiments, the extreme values for the power exponent occur when h=2 mm and γ=0.657 N m^{-1} (upper dashed line, $F_t=17.232U^{2.135}$) and when h=0 mm and γ=0.713 N m^{-1} (lower dashed line, $F_t=3.481U^{1.601}$).

increasing surface tension, γ, from 0.054 to 0.064 N m^{-1}, the power exponent, b, of F_t increases significantly (Fig. 12), as predicted by both the bow wave (equation 2) and surface tension resistance hypotheses (equations 4–7; see also Table 1). None of the simple predictions of the three theories predicted the decrease in b as γ increases from 0.064 to 0.072 N m^{-1}.

The surface of the water downstream from a leg segment was undisturbed, as measured by the flow disturbance index, when U=0, but disturbance of the water surface increased steadily as U increased (Fig. 13). This result supports the hypothesis that drag is operating at all values of U, since the disturbance is an indicator that momentum is being removed from the water by the leg (Fig. 2B). The smooth increase in the index at U from 0 to 0.33 m s^{-1} indicates that there is a continuous transfer of momentum from 0.07 to 0.33 m s^{-1} and

Table 2. *Test for homogeneity of slopes, summary of* F*-values (Type III sums of squares) from an ANOVA performed on the exponents,* b*, of power regression of thrust force,* F_t*, onto relative flow velocity,* U*, in the isolated leg experiments*

Factor	*F*	*P*
h, dimple depth (2)	20.38	0.0001
γ, surface tension (9)	3.36	0.0138

Degrees of freedom (d.f.) are given in parentheses to the right of each factor; error d.f. was 18; sample size was 30.

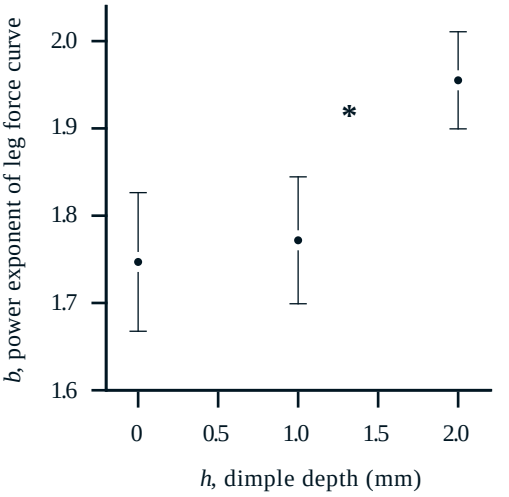

Fig. 11. Dimple depth h and horizontal leg forces. Horizontal forces on an isolated leg segment vary with changes in h. Each point is the mean power exponent, b (see equation 7), for a given value of h (pooled over γ, N=10, means ±1 S.E.M.). Significant differences (*P<0.05) were determined by planned contrasts in an ANCOVA (see Table 3).

that no abrupt alteration in the transfer rate occurs at the velocity at which surface waves begin to form (0.21 m s^{-1}, Fig. 9).

Drag models

At *in vivo* values of U (0.075–0.20 m s^{-1}) and with h=0 and 1 mm, the model of the isolated leg-cum-dimple as a circular cylinder is an excellent predictor of the measured values of F_t, as indicated (a) by a ratio of modeled F_d to measured F_t of 0.80–0.98 (Fig. 14A) and (b) by the estimated values of F_s as

Table 3. *Comparisons using ANCOVA of mean power exponents,* b*, within main experimental effects from the isolated leg experiments*

Contrast	*F*	*P*
0 *versus* 1 mm	0.49	0.4950
1 *versus* 2 mm	26.50	0.0001
0.538 *versus* 0.558 N m^{-1}	0.81	0.3787
0.558 *versus* 0.578 N m^{-1}	0.06	0.8123
0.578 *versus* 0.597 N m^{-1}	3.62	0.0732
0.597 *versus* 0.617 N m^{-1}	1.95	0.1801
0.617 *versus* 0.637 N m^{-1}	5.09	0.0367
0.637 *versus* 0.657 N m^{-1}	0.59	0.4518
0.657 *versus* 0.676 N m^{-1}	1.67	0.2126
0.676 *versus* 0.696 N m^{-1}	0.55	0.4667
0.696 *versus* 0.716 N m^{-1}	2.03	0.1711
0.538 *versus* 0.637 N m^{-1}	6.37	0.0213
0.637 *versus* 0.716 N m^{-1}	17.90	0.0005

These planned contrasts are considered significant when P<0.05.

The broken line delineates contrasts for the independent variables dimple depth (upper) and surface tension (lower).

Degrees of freedom for each contrast was 1.

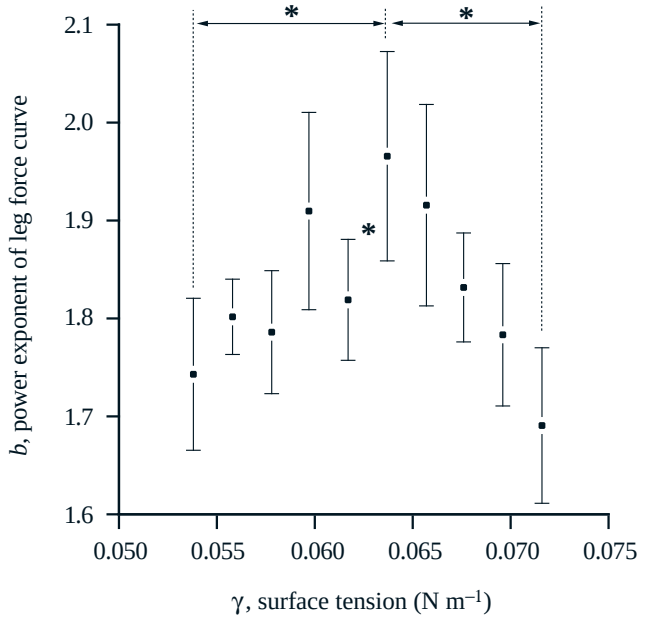

Fig. 12. Surface tension γ and horizontal leg forces. Horizontal forces on an isolated leg segment vary with changes in γ. Each point is the mean power exponent, *b* (see equation 7), for a given value of γ (pooled over *h*, *N*=3, means ±1 S.E.M.). Significant differences (**P*<0.05) were determined by planned contrasts in an ANCOVA (see Table 3). Adjacent means were contrasted, and the two extreme values were individually contrasted with the middle value.

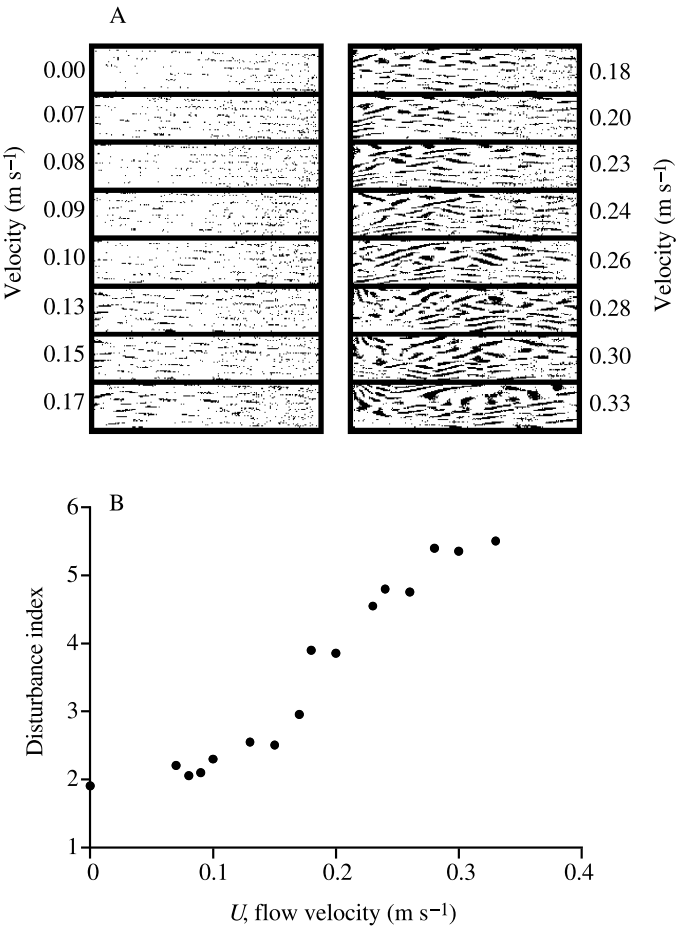

Fig. 13. Flow disturbance behind the leg-cum-dimple *versus* speed. The index of flow disturbance downstream from a leg segment (*l*=10 mm) increases with increasing *U* of the isolated leg segment. Images (A) were produced as described in Fig. 7 and arranged in order of ascending velocity from top to bottom of each column. The corresponding measures of variation in pixel intensity were plotted against velocity (B).

the difference between measured F_t and modeled F_d approached 0 mN (Fig. 14B). The circular cylinder model is less accurate when *h*=2, yielding F_d/F_t ratios of 1.22–1.31 and F_s values of −0.01 to −0.15 mN.

Discussion

Experiments on the isolated legs of *D. triton* demonstrate, for the first time, that drag is the dominant force operating to permit fisher spiders, and quite possibly most other surface-dwelling arthropods, to move horizontally across the water surface. In living spiders, the legs and the dimples they create move backwards at nearly constant velocity, accelerating the body forward in response. The net propulsive force experienced by the spider's body during surface locomotion can be sufficiently explained by the drag forces on the isolated legs, which were measured at *in vivo* flow velocities. Other forces acting on the legs – those due to surface tension and bow wave pressure – appear to be negligible at conditions most closely resembling those seen during non-galloping water surface locomotion in live spiders.

Drag is the primary propulsive force

The bow wave force, F_w, was eliminated as a candidate for the primary source of resistance since waves were not detected behind or in front of the isolated leg at flow velocities, *U*, of 0.20 m s^{-1} or below (Fig. 9). Since the leg tips of live spiders at times move at *U*<0.20 (Fig. 8) and the more proximal portions of the legs move still more slowly, some other resistance mechanism must be operating at low speeds. Most of the resistance is caused by drag, F_d , and not surface tension force, F_s, as indicated by several lines of evidence. First, F_t varied in proportion to *U* to the power 1.601–2.135 (Fig. 10), all values of *b* (see equation 9) within the range seen in a variety of biological systems (Vogel, 1994). The value of *b* alone, however, does not rule out the possibility that surface tension is also providing resistance, since F_s may also increase with the same proportionality to *U* (Table 1). More convincing is the fact that *b* increases significantly as the dimple depth, *h*, increases from 1 to 2 mm; this was the predicted relationship for F_d but not for F_s (Table 1). Furthermore, the significant changes in *b* are due mainly to *h* and not to γ (compare the *F* values in Table 2). At the same time, γ may have an effect on F_t (to be discussed in the next section) as shown by significant changes in *b* with increasing γ (Fig. 12; Table 3).

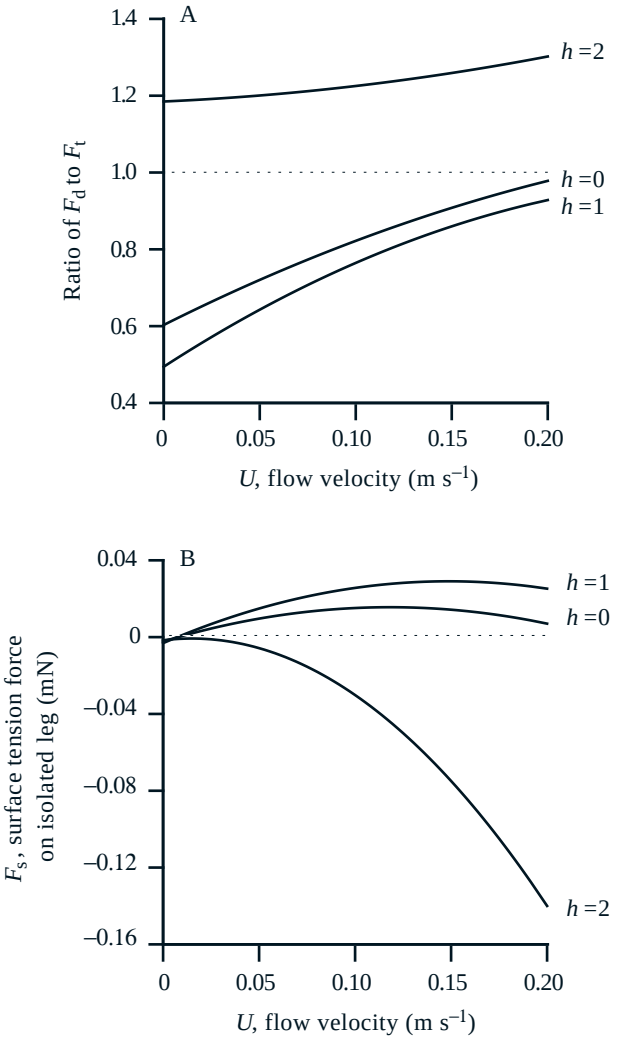

Fig. 14. Drag as a predictor of thrust force, F_t, measured experimentally in isolated legs. The isolated leg was modeled as a circular cylinder, perpendicular to flow, in fresh water at 20 °C; values of drag, F_d, depended on the Reynolds number and dimple depth, h (see equations 11–13). (A) The ratio of F_d to F_t shows that 75–98 % of F_t is predicted by F_d when h=0 and 1 mm and U exceeds 0.075 m s^{-1}; with increasing U, the ratio converges upon 1. When h=2 mm, the ratio of F_d to F_t varies from approximately 1.2 to 1.3 over the entire speed range. (B) The absolute force caused by surface tension, F_s , can be calculated as the difference between F_t and F_d. When h=0 or 1 mm, F_s is small and positive. When h=2, F_s is initially small, but becomes large (in the negative direction) at higher values of U.

Second, a circumstantial piece of evidence supports the primacy of a drag-based mechanism. Flow behind the leg-cum-dimple was disturbed (Fig. 13), relative to still water, at all flow velocities measured (U>0.07 m s^{-1}). Because flow disturbance is evidence that momentum is being transferred from the water to the leg in the sub-surface flow (see Fig. 2B), this photographic assay strongly implicates drag as the source of that flow disturbance.

Third, the modeling of the leg-cum-dimple as a circular cylinder oriented perpendicular to flow (equations 13–15) generates values of F_d that account for 75–98 % of the measured F_t when h=0 or 1 mm and $U \geqslant 0.075$ m s^{-1} (Fig. 14A). This low value for U was half of the lowest *in vivo* value for the leg tip (Fig. 8); parts of the leg in contact with the water, but proximal to the tip, will move more slowly. Note that if only leg tip velocities are used, with a corresponding minimum *in vivo* leg tip velocity of 0.16 m s^{-1}, the drag model is more accurate, accounting for at least 85 % of the measured F_t (Fig. 14A). When the entire range of U is considered ($0 < U \leqslant 0.20$ m s^{-1}), F_s never exceeds values of approximately 0.03 mN when h=1 mm (Fig. 14B). This simple drag model is less accurate when h=2 mm; with that configuration, F_d overestimates F_t by 20–30 % (Fig. 14A).

We do not understand how F_s could be negative when h=2 mm (Fig. 14B). Precise measurements of *in vivo* h and dimple shape (r_a and r_p, α_a and α_p in equations 4–7) might offer an explanation. A negative F_s would actually pull – not resist – the leg, and the dimple geometry required to explain this is $\alpha_a > \alpha_p$ (see Fig. 2C). But this configuration seems unlikely given that the dimple's leading edge cannot travel as a wave and move ahead of the leg, decreasing α_p, since waves are not produced at the speeds we are considering (U<0.20 m s^{-1}). Instead, α_a would have to increase, which could happen if a deep dimple has more vertical walls as the curvature of the surface moves beyond that which can be supported by surface tension (see Denny, 1993). While theoretically possible, such drastic changes in dimple geometry have yet to be visualized. Clearly, dynamic three-dimensional measurements of dimple structure are warranted.

The shape of the dimple may also explain an unpredicted result – the decrease in b with increasing γ approaching that of fresh water (Fig. 12). Recall that our prediction of an increase in F_s (Table 1) was predicated on the assumption that the trailing edge of the dimple would reconfigure such that $\alpha_a < \alpha_p$ (Fig. 2C). The rate of increase in F_t with respect to U would decrease, as indicated by a drop in b (Fig. 12), if α_a increased, decreasing F_s at any given U (assuming a constant F_d), if an increase in γ 'stiffened' the dimple wall.

Propulsion in living spiders

A drag-based mechanism operating at leg speeds, U, below c_{min} (see equation 1) solves Denny's paradox (1993), which states that small or slow-moving surface-dwelling arthropods should not be able to propel themselves horizontally, since their legs would never travel at velocities faster than the 0.23 m s^{-1} needed to create a bow wave and the resulting propulsive force. No such speed limit is imposed on a drag-based mechanism. Thus, the early instars of fisher spiders and water striders are free to locomote across the water surface using legs that never exceed 0.23 m s^{-1}.

The forces experienced by an isolated leg, which are indicative of its propulsive capabilities, are only sufficient to explain surface propulsion in a living spider if the following criteria are met. First, we must rule out propulsive contributions from other structures or mechanisms. Second, we must demonstrate that the isolated legs were tested at

physiological conditions. Third, the forces on an isolated leg must account for approximately half (one of four propulsive legs, usually working in pairs) of the total net force acting on the spider's body. Fourth, the proposed mechanism must be able to account for variation in locomotor speeds seen with changes in size or behavior.

First, the evidence that legs II and III alone are generating thrust comes from the fact that during locomotion they are the only appendages that are in motion relative to the body. A possible propulsive mechanism that would not require leg rowing might include an asymmetric change in γ by the secretion of a surfactant (Denny, 1993). We know of no evidence for this mechanism in spiders. Second, the physiological relevance of these experiments is demonstrated by the fact that we used the isolated leg segment at physiological values of h (see Results) and of U (Fig. 8A).

Third, the maximal thrust force, F_t, measured on the isolated leg was approximately 0.6 mN (Fig. 10), a value within the range of mean body forces measured in live spiders (Fig. 8B). These single leg values are also within the range of horizontal forces measured in single legs of the dead-head cockroach, *B. discoidalis* (Full *et al.* 1995; Full and Ahn, 1995); when adjusted for body mass (kg), one of our spiders, of 0.7 g mass, producing 0.6 mN force with one leg at a leg velocity of $0.2\,m\,s^{-1}$, would generate a mass-specific single leg force of $0.86\,N\,kg^{-1}$, a value close to the horizontal force of a 3 g *B. discoidalis* ($1.7\,N\,kg^{-1}$) during running.

Finally, we can suggest simple ways in which a spider might alter locomotor speeds. First, it can increase the depths of dimples by shifting its weight distribution, which permits larger forces to be applied by the legs to the surface. Second, a spider can alter the angular velocity of its limbs, thus changing the fore-to-aft velocity of the legs and hence drag. Third, it can alter the water-contact length of each leg, thereby altering surface area and drag. By varying the speed and size of the leg-cum-dimple, a spider may also be able to compensate for changes in surface tension that are expected in nature (Denny, 1993). We are pursuing these sources of variability because it is clear that the physics of locomotion at the water surface can only be part of the story for surface-dwelling animals – behavior, especially changes in posture and weight distribution, is likely to be as crucial in this form of locomotion by very small organisms as it is in aerial dispersal by ballooning in spiders (Suter, 1992). We are also pursuing the allometry of the propulsive and glide phases of surface locomotion by measuring the forces acting on first- and later-instar water striders and adult female fisher spiders (a 7000-fold range of masses).

Multiple mechanisms can operate

Finally, it should be noted that in spite of the predominance of drag, the three hypothetical sources of resistance to the motion of a spider's leg at the water surface (Fig. 2; equation 8) are not mutually exclusive. Under some conditions, in fact, all must contribute to the resistance against which a spider or other surface-dwelling arthropod must push when supported by the surface tension of water. For example, when the legs form dimples in the water surface and are moving at velocities greater than $0.23\,m\,s^{-1}$ relative to the water surface, a bow wave will be produced, the moving leg-cum-dimple will encounter some drag, and the dimple will be distorted (Fig. 2). We can also predict the relative importance of the three kinds of resistance under certain conditions: at leg tip velocities less than $0.23\,m\,s^{-1}$, bow waves should be unimportant; at leg tip velocities greater than $0.23\,m\,s^{-1}$ and at dimple depths very close to zero, dimple distortion and drag should be minimized and the relative contribution of bow wave resistance should be maximal; and at dimple depths between 1 and 3.5 mm and velocities below $0.23\,m\,s^{-1}$, drag should predominate. The data presented in this study make possible not only an evaluation of those predictions, but also the conclusion that a single physical process, drag, is ascendant under most conditions.

Appendix

Mathematical symbols used in the text

Symbol	Name	Units	First equation
a	anterior (subscript)	–	4
a	acceleration	$m\,s^{-1}$	–
b	slope of power equation	–	9
c	regression constant	$kg\,s^{-1}$	9
c_{min}	minimum hull speed	$m\,s^{-1}$	1
C_d	drag coefficient	–	–
C_{df}	drag coefficient, frontal	–	3
F	net acceleration force on body	N	–
F_d	drag force on leg	N	3
F_s	surface tension force on leg	N	4
F_t	thrust force on single leg	N	8
F_w	bow wave force on leg	N	2
$\boldsymbol{g}$	gravitational acceleration	$m\,s^{-2}$	1
h	dimple depth	m or mm	6
H	height of wave from trough to peak	m	2
l	length of leg segment	m or mm	4
L_c	characteristic length	m	10
m	mass	kg	–
p	posterior (subscript)	–	5
r	distance from surface to leg contact	m	6
R	resultant of surface tension force	N	–
Re	Reynolds number	–	10
S_f	surface area, frontal	m^2	2
U	velocity of flow or leg	$m\,s^{-1}$	2
x	regression variable	$m\,s^{-1}$	9
y	regression variable	N	9

Symbol	Name	Units	First equation
α	orientation of *R* to water surface	degrees	5
β	angle in Fig. 5	degrees	–
γ	surface tension	$N\,m^{-1}$ or $J\,m^{-1}$	1
λ	wavelength	m	2
ν	kinematic viscosity	$m^2\,s^{-1}$	10
ρ	density of the fluid	$kg\,m^{-3}$	1

We thank Edgar Leighton at the University of Mississippi for providing us with the subjects of this study, Erin Murphy for some of the data collection, Pam Murphy for some of the spider illustrations, and two anonymous reviewers for their careful and very constructive comments on an earlier version of the manuscript. The study was supported in part by funds provided by Vassar College through both the Undergraduate Research Summer Institute and the Class of '42 Faculty Research Fund. J.H.L. was funded by the Office of Naval Research (Grant N00014-97-1-0292).

References

ALEXANDER, R. MCN. (1977). Mechanics and scaling of terrestrial locomotion. In *Scale Effects in Animal Locomotion* (ed. T. J. Pedley), pp. 93–110. New York: Academic Press.

ALEXANDER, R. MCN. (1989). Optimization and gaits in the locomotion of vertebrates. *Physiol. Rev.* **69**, 1199–1227.

ANDERSON, N. M. (1976). A comparative study of locomotion on the water surface in semiaquatic bugs (Insects, Hemiptera, Gerromorpha). *Vidensk. Meddr. dansk. naturh. Foren.* **139**, 337–396.

BARNES, W. J. P. AND BARTH, F. G. (1991). Sensory control of locomotor mode in semi-aquatic spiders. In *Locomotor Neural Mechanisms in Arthropods and Vertebrates* (ed. D. M. Armstrong and B. M. H. Bush), pp. 105–116. Manchester: Manchester University Press.

BLICKHAN, R. AND FULL, R. J. (1993). Similarity in multilegged locomotion: bouncing like a monopode. *J. comp. Physiol.* **173**, 509–517.

BOWDAN, E. (1978). Walking and rowing in the water strider, *Gerris remigis*. I. A cinematographic analysis of walking. *J. comp. Physiol.* **123**, 43–49.

CHEMICAL RUBBER COMPANY (1993). *CRC Handbook of Chemistry and Physics.* Cleveland: CRC Press.

DANIEL, T. L. (1984). Unsteady aspects of aquatic locomotion. *Am. Zool*. **24**, 121–134.

DENNY, M. W. (1993). *Air and Water: The Biology and Physics of Life's Media*. Princeton: Princeton University Press.

DESHEFY, G. S. (1981). 'Sailing' behaviour in the fishing spider, *Dolomedes triton* (Walckenaer). *Anim. Behav*. **29**, 965–966.

FARLEY, C. T. AND MCMAHON, T. A. (1992). Energetics of walking and running: insights from simulated reduced-gravity experiments. *J. appl. Physiol*. **73**, 2709–2712.

FARLEY, C. T. AND TAYLOR, C. R. (1991). A mechanical trigger for the trot–gallop transition in horses. *Science* **253**, 306–308.

FEDAK, M. A., HEGLUND, N. C. AND TAYLOR, C. R. (1982). Energetics and mechanics of terrestrial locomotion. II. Kinetic energy changes of the limbs and body as a function of speed and body size in birds and mammals. *J. exp. Biol*. **79**, 23–40.

FULL, R. J. (1990). Concepts of efficiency and economy in land locomotion. In *Concepts of Efficiency and Economy in Animal Physiology* (ed. R. W. Blake), pp. 97–131. New York: Cambridge University Press.

FULL, R. J. AND AHN, A. N. (1995). Static forces and moments generated in the insect leg: comparison of a three-dimensional musculo-skeletal computer model with experimental measurements. *J. exp. Biol*. **198**, 1285–1298.

FULL, R. J. AND TU, M. S. (1991). Mechanics of a rapid running insect: two-, four- and six-legged locomotion. *J. exp. Biol.* **156**, 215–231.

FULL, R. J., YAMAUCHI, A. AND JINDRICH, D. L. (1995). Maximum single leg force production: cockroaches righting on photoelastic gelatin. *J. exp. Biol*. **198**, 2441–2452.

GERTSCH, W. J. (1979). *American Spiders* (2nd edn). New York: Van Nostrand Reinhold Company.

GLASHEEN, J. W. AND MCMAHON, T. A. (1996*a*). A hydrodynamic model of locomotion in the Basilisk lizard. *Nature* **380**, 340–342.

GLASHEEN, J. W. AND MCMAHON, T. A. (1996*b*). Size-dependence of water-running ability in basilisk lizards (*Basiliscus basiliscus*). *J. exp. Biol.* **199**, 2611–2618.

GORB, S. N. AND BARTH, F. G. (1994). Locomotor behavior during prey-capture of a fishing spider, *Dolomedes plantarius* (Araneae: Araneidae): Galloping and stopping. *J. Arachnol*. **22**, 89–93.

KRAM, R., DOMINGO, A. AND FERRIS, D. P. (1997). Effect of reduced gravity on the preferred walk–run transition speed. *J. exp. Biol*. **200**, 821–826.

MCALISTER, W. H. (1959). The diving and surface-walking behaviour of *Dolomedes triton sexpunctatus* (Araneida: Pisauridae). *Anim. Behav*. **8**, 109–111.

SCHMIDT-NIELSEN, K. (1984). *Scaling: Why is Animal Size so Important?* Cambridge: Cambridge University Press.

SHULTZ, J. W. (1987). Walking and surface film locomotion in terrestrial and semi-aquatic spiders. *J. exp. Biol.* **128**, 427–444.

SOKAL, R. R. AND ROHLF, F. J. (1981). *Biometry: The Principles And Practice of Statistics in Biological Research* (2nd edn). New York: W. H. Freeman and Company.

SUTER, R. B. (1992). Ballooning: Data from spiders in freefall indicate the importance of posture. *J. Arachnol.* **20**, 107–113.

VOGEL, S. (1994). *Life in Moving Fluids* (2nd edn). Princeton: Princeton University Press.